Aiming to Complex Power Quality Disturbances: A Novel Decomposition and Detection Framework

# Aiming to Complex power quality disturbances: A Novel Decomposition and Detection Framework

Kunzhi Zhu, Zhaosheng Teng, Wei Qiu, *Member, IEEE*, Alessandro Mingotti, *Member, IEEE*, Qiu Tang, Wenxuan Yao, *Senior Member, IEEE*

***Abstract*— In recent years, due to the penetration of renewable energy and the widespread use of power electronic equipment, power quality disturbances (PQDs) have become more complex and hazardous. As the premise of power quality control, complex PQDs require more accurate and efficient detection. To address this issue, this paper proposes a novel automatic method for detecting complex PQDs based on integrated intrinsic variable time scale decomposition (I-IVTD) and weighted recurrent layer aggregation network (WRLA). The proposed I-IVTD method reduces aliasing and endpoint effects, and improves anti-noise performance by innovative use of variable time scales and multiple integrations. The improved WRLA network enhances learning ability and accelerates convergence by adding three weights to each unit. The proposed framework can effectively detect 27 complex disturbances automatically and does not require manual feature design. Finally, a large number of experiments are conducted, including simulation experiments and tests on a PQDs analysis platform. The test results based on the analysis platform indicate that the accuracy for complex disturbances is higher than 98 %, which demonstrates the superior performance of the proposed framework. Notably, it is effective for detecting nonlinear disturbances as well.**

***Index Terms*— Complex power quality disturbances (PQDs), Integrated intrinsic variable time scale decomposition (I-IVTD), Weighted recurrent layer aggregation networks (WRLA)**

## I. Introduction

RECENTLY, the penetration of renewable energy is growing rapidly [1]. However, due to the unstable and randomness of renewable energy and the application of a large number of power electronic equipment, power quality disturbances (PQDs) are becoming more complex and hazardous. These complex PQDs can interfere with the operation of precision equipment and affect the stability of the power grid [2], even causing economic losses [3]. According to IEEE-1159 standard [4], 9 types of single disturbances are defined. However, steady-state disturbances such as harmonics and flicker could persist for a long time, while voltage dips and transients only exist for a short period. Therefore, different disturbances may occur simultaneously to form complex disturbances. Due to the complexity and diversity of complex PQDs signals, it is more difficult to accurately detect. As the premise of power quality control, accurate detection of complex PQDs is more challenging and necessary than single disturbances.

In general, power quality detection consists of signal preprocessing and classification. For the convenience of understanding, existing frameworks are introduced based on this narrative logic. It should be noted that the introduction includes both methods applied in the traditional power grid and renewable energy scenarios. In the first stage, the fast Fourier transform (FFT) is the basic spectrum analysis method. However, FFT is only applicable to extract spectral features [5] and analyze power system parameters [6]. The short-time Fourier transform (STFT) is used to process PQDs signals [7] as it increases the feature dimension. However, STFT is not sensitive to mutation signals that are smaller than the window width. Discrete wavelet transformation (DWT) and Stockwell transform (ST) are also applied to power quality detection [8] [9] [10] [11]. Unlike STFT and DWT, ST has variable time-frequency resolution, but the time-frequency resolution is not self-adaptive. Different from DWT and ST, hilbert huang transform (HHT) [12], ensemble empirical mode decomposition (EEMD) [13] and variational mode decomposition (VMD) [14] [15] are self-adaptive decomposition methods, they are also widely used in power quality detection. Although EEMD and VMD have better anti-noise performance, endpoint effects and mode aliasing are unavoidable [16]. The fast independent component analysis (FICA) is also used for disturbance identification under strong noise [17], but FICA is only used for denoising, and signal features still need to be further extracted. Singular value decomposition (SVD) [18] and instantaneous frequency estimation (IFE) are also applied to power quality analysis

This work is supported by the National Natural Science Foundation of China under Grant 52077067 and Hunan Natural Science Foundation 2021JJ30124, and in part by the China Postdoctoral Science Foundation under number BX20220102 and 2022M721084, and in part by the Changsha National Natural Science Foundation under number kq2208027. *(Corresponding author: Zhaosheng Teng.)*

K. Zhu, Z. Teng, W. Qiu, Q. Tang, and W. Yao are with the College of Electrical and Information Engineering, Hunan University, Changsha 410082, China. And K. Zhu also with the Department of Electrical, Electronic and Information, University of Bologna, Bologna 40136, Italy. (e-mail: zhukunzhi@hnu.edu.cn; tengzs@hnu.edu.cn; qiuwei@hnu.edu.cn; tangqiu@hnu.edu.cn; wenxuanyao@hnu.edu.cn).

A. Mingotti is with the Department of Electrical, Electronic and Information, University of Bologna, Bologna 40136, Italy (e-mail: alessandro.mingotti2@unibo.it).

[19] and detection [20]. Although SVD can reduce the size of the feature map, it is difficult to determine the effective singular value. IFE is suitable for non-stationary signals, but it needs to calculate the instantaneous frequency and perform the signal compression transformation after performing the time-frequency transformation, so its computational complexity still needs to be reduced.

In the stage of disturbance detection, machine learning methods are the general trend. Machine learning does not rely on mathematical models and can learn from training data independently. An artificial neural network (ANN) is used for single and combined power quality disturbances detection in [5] and [21]. Decision tree (DT) [15], support vector machine (SVM) [22], random forest (RF) [23], and improved k-nearest neighbor (KNN) [24] are also applied in PQDs detection. However, limited by the performance of traditional machine learning methods, these frameworks require manual design features, which means that they rely on expert experience. With the rapid development of the convolutional neural network (CNN), it is widely used in PQDs detection due to its stronger feature learning ability. In [25], a three-level multiply connected Bayesian network (TLBN) is proposed to classify PQDs, and the deep convolutional neural network (DCNN) is also applied in [26]. In [27], a typical network structure of the residual neural network (ResNet) is used. In [28], the correlation between PQDs is considered and a detection method based on bidirectional recurrent neural models is proposed. The generative adversarial network (GAN) is also applied to PQDs identification in data loss scenario [29]. In [30], the explainability of the classifier is considered by using explainable artificial intelligence (XAI). Although the above frameworks have achieved passable results, most of them focus on the design of classifiers and ignore the pre-processing of signals, which will lead to information loss and affect the robustness of the framework. With the development and extensive application of new energy, power quality disturbances are becoming more and more complex, which challenges the accurate detection of PQDs.

To improve the effectiveness of complex power quality disturbances detection, this paper proposes a novel detection framework. The contributions of this paper are outlined below:

1) To fully utilize information in the PQDs signal, the integrated intrinsic variable time scale decomposition (I-IVTD) is proposed. The advantage of I-IVTD is that it avoids repeated decomposition through the variable time scale mechanism, which reduces modal aliasing. And it also reduces the endpoint effect and improves anti-noise performance by incorporating Gaussian noise and multiple integration mechanisms. Additionally, the paper provides a selection method for key parameters of I-IVTD.
2) To accurately detect complex power quality disturbances, an improved weighted recurrent layer aggregation network (WRLA) is proposed. WRLA enhances the feature learning ability of the network by giving different weights to the feature maps. Compared to recurrent layer aggregation networks (RLA), WRLA reduces the parameter amount while ensuring performance.
3) A novel complex PQDs detection framework is proposed based on I-IVTD and WRLA networks. The framework is automatic and does not rely on expert experience to manually design features. It reduces redundant parameters by adjusting the structure of the deep network. Experiments show that the proposed framework has high detection accuracy and strong anti-noise performance.
4) To verify the validity of the proposed framework, a real-time detection system for complex PQDs is designed. The tests on experimental platforms proved the effectiveness of the proposed framework.

The paper is organized as follows: Section II presents the principle and performance comparison of I-IVTD, and Section III introduces the proposed WRLA. Section IV proposes the I-IVTD & WRLA framework, and Section V shows the experiments. Finally, Section VI presents the conclusion.

## II. Proposed I-IVTD method

Feature extraction plays a crucial role in accurately detecting complex PQDs signals. In 2007, Frei and Osorio introduced the intrinsic time scale decomposition (ITD) method [31], which decomposes signals into a combination of baseline and proper rotation components. Due to its efficiency and effectiveness, ITD has significant potential for various applications. However, its performance is limited by mode aliasing and the endpoint effect. In order to overcome these limitations, the Integrated Intrinsic Variable Time Scale Decomposition method is proposed in this paper.

### A. Principle of I-IVTD

In the proposed I-IVTD, the variable time scale and the multi-integration are its unique characteristics. Defining the discrete PQDs signals as $x(t)$, and the number of integrations as $J$, the decomposition process of I-IVTD is shown as follows.

1) First, Gaussian noise $g(t)$ is generated, the length of $g(t)$ is equal to $x(t)$ and its amplitude is $P$. Add $g(t)$ to $x(t)$, it can be expressed as

$$X(t) = x(t) + g(t). \tag{1}$$

The purpose of this step is to adjust the local extreme point changes caused by the original noise in the signal.

2) Then search the local extremum of $X(t)$ and record as $X(\tau_m), (m = 1, 2, 3, ..., M)$, where the minimum distance between $X(\tau_m)$ meets $Mind_1 > 0$ and $\tau_m$ is the time corresponding to the $X(\tau_m)$, definition $\tau_0 = 0$. When $t \in [\tau_m, \tau_{m+2}]$, the baseline signal $L(t)$ is defined as

$$L(t) = L_m + \left(\frac{L_{m+1} - L_m}{X(\tau_{m+1}) - X(\tau_m)}\right)(X(t) - X(\tau_m)), \quad t \in (\tau_m, \tau_{m+1}], \tag{2}$$

where, $L_0$ and $L_{m+1}$ is defined as

$$\begin{cases} L_0 = (X(\tau_0) + X(\tau_1))/2, \\ L_{m+1} = \\ \alpha\left[X(\tau_m) + \left(\dfrac{\tau_{m+1} - \tau_m}{\tau_{m+2} - \tau_m}\right)(X(\tau_{m+2} - X(\tau_m))\right] \\ + (1-\alpha)X(\tau_{m+1}), \alpha \in (0,1). \end{cases} \tag{3}$$

In Equation (3), the value of $\alpha$ is typically taken as 0.5.

3) It can be found that $L(t)$ is a linear transformation of $X(t)$, it represents the low-frequency component of the original signal, the high-frequency component ("proper rotation") $H_1(t)$ is defined as

$$H_1(t) = X(t) - L(t). \tag{4}$$

4) After obtaining $H_1(t)$, take $L(t)$ as the signal to be decomposed, repeat steps (2)-(3), and the signal can be decomposed continuously. Differently from ITD, I-IVTD uses variable time scales to search for the local maximum point of the signal according to the following equation:

$$\begin{cases} Mind_1 > 0, \\ Mind_k > Maxd_{k-1}, (k > 1, k \in \mathbb{N}), \end{cases} \tag{5}$$

where $Mind_k$ represents the minimum distance between local extreme points of the signal in the $k$-th decomposition, and $Maxd_{k-1}$ represents the maximum distance between local extreme points which were previously searched. The purpose of this step is to skip scales that have already been extracted.

5) When the stop condition is met, the decomposition will stop. Setting the stop condition to $L(t)$ is monotone or the amplitude of $L(t)$ is less than the threshold. Assume that the signal is decomposed $K$ times, $X(t)$ can be written as:

$$X(t) = \sum_{k=1}^{K} H(t)_k + L(t). \tag{6}$$

As I-IVTD employs the variable time scale mechanism in its search for local extreme points of signals, it prevents redundant searching for the same time scale, and thus reduces mode aliasing. Fig. 1 illustrates the decompose details of ITD and I-IVTD.

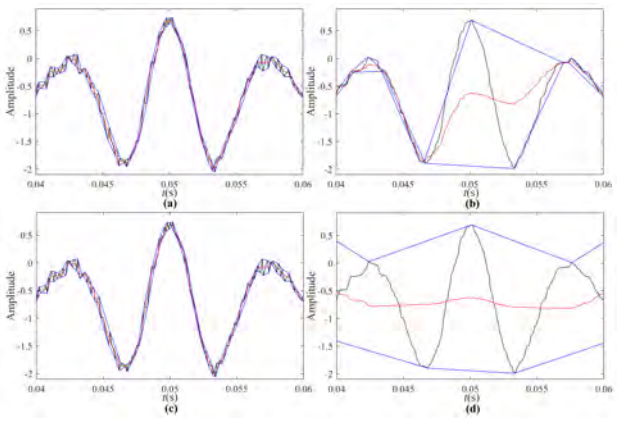

Fig. 1. Decompose details of ITD and I-IVTD.

where, (a) and (c) is the first decomposition of ITD and I-IVTD respectively, (b) and (d) is the second decomposition of ITD and I-IVTD. The black line denotes the signal waveform, the blue line represents the connection between local maximum and local minimum, and the red line signifies the decomposed L(t). Upon comparing (a) and (c), it can be observed that the first decomposition of ITD and I-IVTD are identical. However, with the second decomposition, I-IVTD mitigates mode aliasing by utilizing variable time scale.

6) Finally, to integrate multiple decompositions, repeat steps (1)-(5) $J$ times, and use zero filling to align the decomposition results, so that the number of all decomposed components remains the same, and then take the average value of the corresponding components. Hence:

$$\begin{cases} L(t) = \frac{1}{J}\sum_{j=1}^{J} L(t)^j, \\ H(t)_k = \frac{1}{J}\sum_{j=1}^{J} H(t)_k^j, (k = 1, 2, \ldots, K). \end{cases} \tag{7}$$

It is important to note that during this step, Gaussian noise is added to the signal before each decomposition in an independent and identically distributed manner. This introduces slight variations in the results of each decomposition. However, the added Gaussian noise is almost eliminated during the averaging process, and the integration of multiple decomposition results enhances the anti-noise performance of I-IVTD.

### *B. Parameter selection of I-IVTD*

In I-IVTD, the amplitude of the added Gaussian noise $P$ and the number of integrations $J$ are two key parameters. An optimal $P$ value should satisfy two objectives: adjusting the local extreme point change caused by noise in the original signal and not inducing additional decomposition errors. Moreover, the value of $J$ is directly proportional to the computational effort. Therefore, $J$ needs to be appropriately selected to limit the decomposition errors resulting from added Gaussian noise and to ensure that the computational effort is acceptable. In this paper, we use a typical nonlinear signal, frequency modulation and amplitude modulation (FM-AM) signal $S(t)$, to determine the key parameters of I-IVTD. $S(t)$ is defined as:

$$S(t) = G_n(t) + d_1(t) + d_2(t), \tag{8}$$

where, $G_n(t)$ represents the original noise in the signal. The signal-to-noise ratios (SNR) of $S(t)$ can be changed by adjusting the amplitude of $G_n(t)$. $d_1(t)$ and $d_2(t)$ are defined as follows:

$$\begin{cases} d_1(t) = \sin(2\pi 5t)\sin(2\pi 15t), \\ d_2(t) = (1 + 0.5\cos(2\pi 60t))\cos(2\pi 100t + 2\sin(2\pi 20t)). \end{cases} \tag{9}$$

where, the signal duration is 0.2 s and the sampling frequency is 10 kHz. It should be noted that the parameters of $s(t)$ should be random to ensure representativeness. Considering

that I-IVTD is based on time-domain linear transformation, the Pearson correlation coefficient $\rho$ is used to measure the effectiveness of decomposition. For convenience, all decomposed levels are recorded as $L_i(i = 1, 2, ..., q)$, then the correlation between $L_i$ and the original signal $S(t)$ can be calculated with the following equation:

$$\rho = \frac{1}{q}\sum_{i=1}^{q}\frac{\mathrm{cov}(S(t), L_i)}{\sigma_{S(t)}\sigma_{L_i}}, \tag{10}$$

where, $\mathrm{cov}(S(t), L_i)$ is the covariance of $S(t)$ and $L_i$, $\sigma_{S(t)}$ and $\sigma_{L_i}$ is their standard deviation.

To better select the key parameters, we utilize the control variable method. Initially, $J$ is set to a sufficiently large value to achieve an ideal influence. Next, we add Gaussian noise with various $P$ values to $S(t)$ and determine the optimal $P$ value based on the Pearson correlation coefficient. In this step, we set $J$ to 100 and adjust the amplitude of the added noise, $P$. The SNR of the tested signal ranges from 20 dB to 60 dB in increments of 10 dB, while the added noise amplitude varies from 0.01 to 0.1 per unit (p.u.) in increments of 0.01 p.u. The test results are illustrated in Fig. 2.

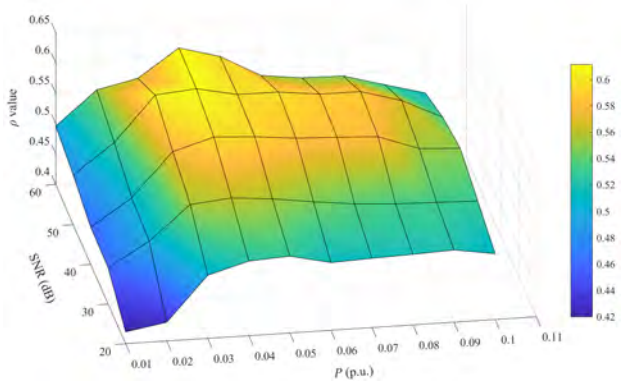


Fig. 2. $\rho$ value trend under different $P$.

As depicted in Fig. 2, for a given $P$ value, $\rho$ increases as the signal's SNR becomes higher. This is because the presence of less noise in the original signal makes I-IVTD more effective. When $P$ changes from 0.01 p.u. to 0.1 p.u., $\rho$ initially increases and then decreases. The reason for this is that a small $P$ value cannot effectively alter the local extreme points of the signal but when $P$ is greater than 0.06 p.u., the added Gaussian noise will cause an obvious decomposition error. From the changing trend of $\rho$, it can be found that I-IVTD performs best at $P = 0.04$, so it is selected as the optimal value.

Once the optimal $P$ value is obtained, we determine the integrated number $J$. As the $J$ value increases, the decomposition error caused by the added Gaussian noise decreases. However, this is accompanied by a linear increase in the computational cost. Thus, it is necessary to strike a balance between the decomposition error and the computational burden. To meet the real-time requirements of complex PQDs detection, we test the $J$ values ranging from 10 to 50, and the results are presented in Table I. It can be found that the value of $\rho$ increases fastest when $J$ is from 10 to 20, and then the growth rate slows down. Finally, $J$=20 is taken as the optimal value.

TABLE I
$\rho$ VALUE UNDER DIFFERENT $J$

| Integrated number ($J$) | $\rho$ | | | | |
|---|---|---|---|---|---|
| | 20 dB | 30 dB | 40 dB | 50 dB | 60 dB |
| 10 | 0.5214 | 0.5478 | 0.5573 | 0.5601 | 0.5751 |
| 20 | 0.5308 | 0.5645 | 0.5676 | 0.576 | 0.5913 |
| 30 | 0.535 | 0.5679 | 0.5682 | 0.5785 | 0.5935 |
| 40 | 0.5385 | 0.5687 | 0.5739 | 0.5798 | 0.5987 |
| 50 | 0.5399 | 0.5704 | 0.5765 | 0.5846 | 0.6016 |

### C. Performance comparison with ITD

In this part, the decomposition results of I-IVTD and ITD are shown in the same figure to compare their performance visually.

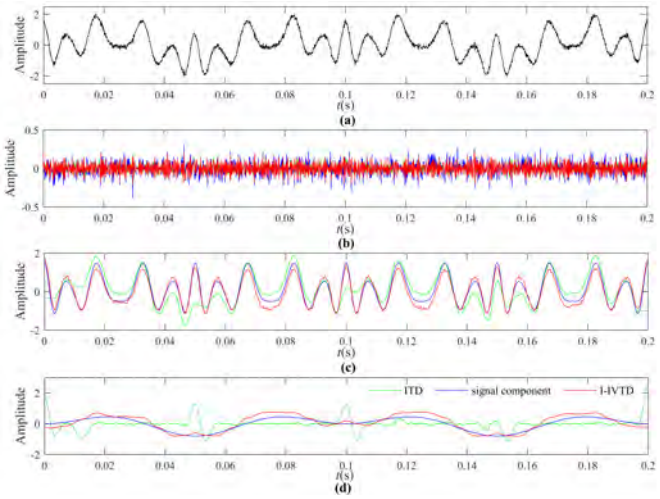


Fig. 3. Decomposition results of ITD and I-IVTD. (a) Waveform of $S(t)$. (b) $G_n(t)$ and $H_1(t)$. (c) $d_1(t)$ and $H_2(t)$. (d) $d_2(t)$ and $L(t)$.

In Fig.3, the SNR of $S(t)$ is 20 dB. It can be found that compared with ITD, I-IVTD performs better in modal aliasing because the variable time scale of I-IVTD avoids repeated decomposition of the same scale. At the same time, the error of I-IVTD at the endpoint is smaller. The reason is that the multiple integration mechanism of I-IVTD inhibits the endpoint effect. This test uses a signal with SNR of 20 dB, which also means that I-IVTD performs better than ITD under strong noise.

## III. PROPOSED WEIGHTED RECURRENT LAYER AGGREGATION NETWORK

To accurately detect complex power quality disturbances, this section proposes an improved machine learning method: the weighted recurrent layer aggregation network.

### A. Structure of RLA

Machine learning has become increasingly prevalent in the analysis of complex power quality disturbances. There are two typical types of networks used in machine learning methods: feedforward neural networks (FNN) and recurrent neural networks (RNN). FNNs excel at extracting features from single inputs, while RNNs possess memory capabilities and

can learn correlations between different inputs. The recurrent layer aggregation network (RLA) [32] is a lightweight module that combines the principles of FNNs and RNNs by introducing the concept of layer aggregation. RLA can be combined with existing convolutional neural networks (CNNs) to enhance the network's feature extraction ability. A schematic diagram of RLA is shown in Fig. 4.

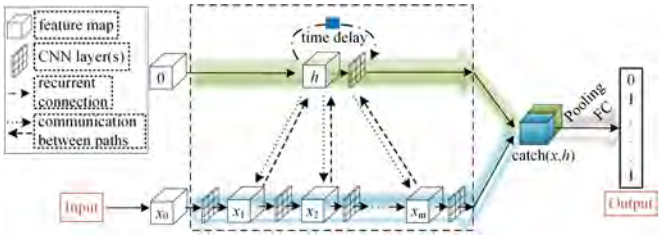


Fig. 4. The schematic diagram of RLA module.

In Fig. 4, $x$ represents the hidden feature map in CNN, and $h$ is the hidden state. At different stages of CNN, information will be exchanged with $h$ by layer aggregation. Because the history information of different hidden feature maps of CNN is stored in $h$, this process can improve the information exchange within CNN and strengthen the feature extraction ability.

### B. Structure of the Proposed WRLA unit

In [32], the authors list six kinds of network structures based on ResNet-50 and the concept of layer aggregation. The per-test shows that RLA-V6 performs best in complex power quality detection and the structure of RLA-V6 is shown in Fig. 5(a).

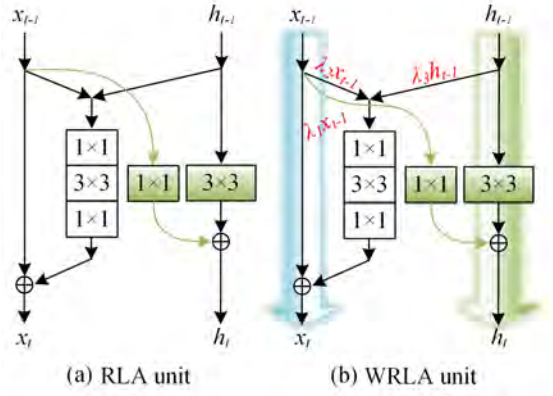


Fig. 5. The structure of RLA and WRLA unit.

From Figure 5(a), it can be observed that the different feature maps are fused with equal weight. However, in reality, the influence of each feature map may not be equal. Taking this into consideration, the Weighted Recurrent Layer Aggregation (WRLA) unit is proposed, and its structure is illustrated in Fig. 5(b). In WRLA unit, the mapping functions of $X_t$ and $h_t$ become:

$$\begin{cases} x_{(t)} = \lambda_1 x_{(t-1)} + f_1(\lambda_2 x_{(t-1)}, \lambda_3 h_{(t-1)}), \\ h_{(t)} = f_2(x_{(t-1)}, h_{(t-1)}), \\ s.t. \lambda_1 + \lambda_2 + \lambda_3 = 3. \end{cases} \tag{11}$$

where, $\lambda_1, \lambda_2, \lambda_3 \in (0, 3)$ and their initial values are set to 1. It can be found that there is no difference between RLA and WRLA in the initial state. But with the training of the network, $\lambda_1, \lambda_2, \lambda_3$ will be automatically updated through a gradient descent method to weighting different feature maps, which makes WRLA further enhances feature extraction and accelerates convergence.

## IV. Complex PQDs detection framework based on I-IVTD and WRLA network

In this section, we propose a complex PQDs detection framework based on the I-IVTD & WRLA network. The framework is divided into two parts: complex PQDs signal decomposition and detection. Unlike the common PQDs detection framework, this approach does not require manual design features such as skewness or kurtosis of the signal [22].

In the first part, the complex PQDs signal is decomposed using I-IVTD into $8 \times 640$ matrices, which are then downsampled to $8 \times 320$. Downsampling is performed to reduce the network burden, while a higher sampling rate benefits the I-IVTD process. The data is normalized and fed into the WRLA network.

In the second part, the structure and parameters of the WRLA network need to be determined. For instance, smaller kernel sizes are beneficial for capturing details but lack receptive fields, while larger kernel sizes enhance the receptive field but increase the number of parameters. Deeper networks can improve feature extraction but risk overfitting. On the other hand, it is necessary to redesign the depth of the network and the number of channels in the convolutional layer. The advantage of this operation is that it can further reduce network parameters. To address these issues, we use the grid search method, and the structure of the framework is shown in Figure 6.

Figure 6 shows multiple WRLA units with the same channel described as a 'stage'. The number of WRLA units for stages 1, 2, and 3 is 3, 4, and 6, respectively. '$C_1$' and '$C_2$' denote the number of channels for $x_t$ and $h_t$, respectively. It should be noted that due to the stronger feature extraction ability of WRLA, the performance of WRLA is better compared to RLA with the same number of parameters. If increase the depth or the number of channels in the convolutional layer of RLA, it can also achieve similar performance as WRLA, but the cost is to increase the number of parameters. Under the premise of similar performance (accuracy difference less than 0.1 %), WRLA reduced 77.4 thousand parameters.

## V. Experiments and Analysis

In this section, several experiments are described to verify and compare the performance of the proposed framework. The CPU and GPU used in the experiment are the i5-8300h and the GTX1050 respectively.

### A. Test data of complex PQDs

According to IEEE-1159 standards [4] and [33], nine single PQDs signals and sixteen complex disturbances are generated. Additionally, this paper considers two types of non-linear disturbances to enhance the robustness of the proposed framework, including voltage transients with swells

and voltage flicker with transients. The non-linear disturbance is generated by modulating different disturbance signals, and the basis for this consideration is that different disturbances occurring simultaneously can mix in modulation. Finally, all disturbances are listed in Tab. II.

TABLE II
ALL PQD SIGNALS

| Class | PQ disturbance | Class | PQ disturbance |
|---|---|---|---|
| C1 | Normal | C15 | Sag + transient |
| C2 | Swell | C16 | Spike + transient |
| C3 | Sag | C17 | Transient + harmonics + sag |
| C4 | Interrupt | C18 | Transient + harmonics + swell |
| C5 | Transient | C19 | Transient + harmonics + interrupt |
| C6 | Flicker | C20 | Transient + harmonics + flicker |
| C7 | Harmonics | C21 | Flicker + harmonics + interrupt |
| C8 | Notch | C22 | Flicker + harmonics + swell |
| C9 | Spike | C23 | Flicker + harmonics + sag |
| C10 | Swell + harmonics | C24 | Notch + transient + swell |
| C11 | Sag + harmonics | C25 | Spike + transient + swell |
| C12 | Flicker + harmonics | **C26** | **Transient with swell** |
| C13 | Interrupt + harmonics | **C27** | **Flicker with transient** |
| C14 | Swell + transient | | |

The simulation signal is generated in MATLAB with a sampling rate of 3.2 kHz, and the number of sampling points is 640. Each disturbance randomly generates 2000 samples that differ from each other, with 60 % as the training set, 20 % as the validation set, and 20 % as the testing set. Gaussian noise will also be added to the signal during the experiment to alter the signal-to-noise ratio.

### B. Performance under different SNR

Considering the fact that the SNR of the signal changes over time, this section tests the performance of the frameworks under different SNRs, and the results are listed in Table III.

Table III shows that decreasing SNR reduces detection accuracy, but the proposed framework consistently achieves high accuracy under different SNRs due to I-IVTD's superior anti-noise performance. Even at 20 dB, the proposed framework still has an accuracy of 98.71 %. Comparing

TABLE III
COMPARISON BEFORE AND AFTER IMPROVEMENT

| Framework | Accuracy(%) | | | | Test time per sample (ms) |
|---|---|---|---|---|---|
| | 20 dB | 30 dB | 40 dB | clear | |
| ITD & RLA | 96.04 | 96.95 | 97.46 | 97.95 | 4.73+0.569 |
| ITD & WRLA | 96.88 | 97.52 | 97.92 | 98.33 | 4.73+0.63 |
| I-IVTD & WRLA | 98.71 | 99.06 | 99.35 | 99.52 | 97.65+0.63 |

WRLA and RLA, WRLA only adds three parameters per unit than RLA, but has an 0.84 % improvement in accuracy when SNR is 20 dB. While the cost of I-IVTD is a longer running time, it still detects complex PQDs in real-time because the PQDs signal's sampling duration is 200 ms.

Table IV lists the accuracy of each disturbance under 20 dB. Overall, ITD & RLA performs worst, ITD & WRLA is better, and I-IVTD & WRLA is the best. For some single disturbances, their performance is similar as these disturbances are easier to detect. For most complex disturbances, the accuracy of the proposed framework is higher than 98 %. In particular, the proposed framework has a clear advantage in detecting nonlinear disturbances because I-IVTD is more effective for nonlinear signals, and the improved WRLA network has stronger learning abilities.

### C. Comparison with different feature extraction and classifier methods

To verify the performance of the proposed I-IVTD & WRLA framework, this section compares it with different feature extraction and classifier methods. Similar to ITD, both VMD and EEMD is adaptive feature extraction methods. VMD estimates signal components using the Lagrange multiplier method, while EEMD filters the intrinsic mode function by calculating the mean value of the boundary envelope. To ensure a fair comparison, the ensemble number of EEMD is the same as that of I-IVTD, and the feature map size of VMD and EEMD is set to $8 \times 320$. Additionally, different classifiers are set to the same number of layers and nodes. The SNR of the test signal is 20 dB, and the accuracy trend of different frameworks during the training process is shown in Fig. 7.

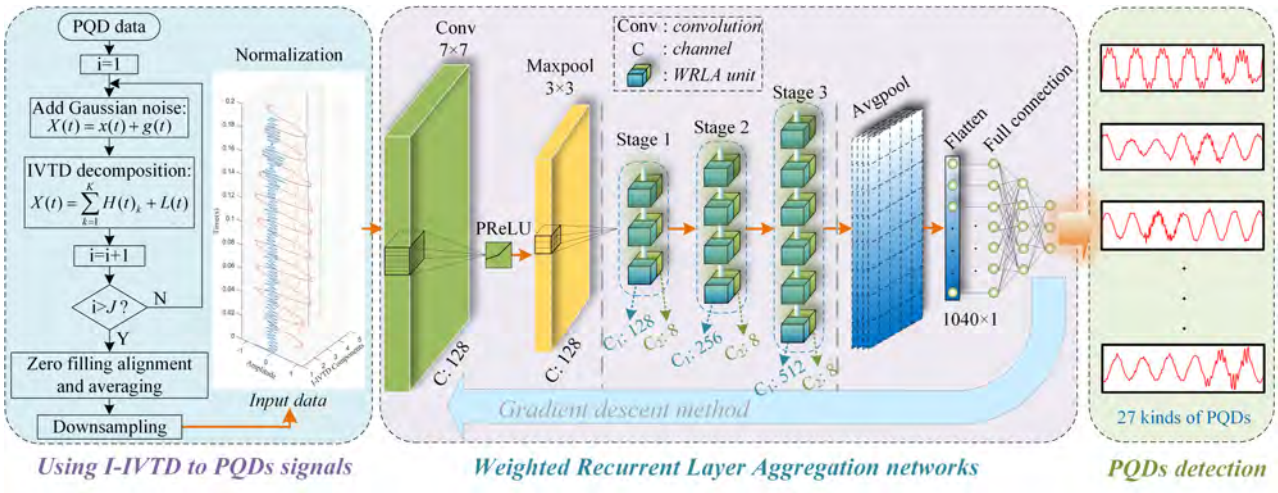


Fig. 6. The structure of the proposed framework.

TABLE IV
PERFORMANCE OF EACH PQD UNDER 20DB

| Class | Accuracy(%) | | |
|---|---|---|---|
| | ITD&RLA | ITD&WRLA | I-IVTD&WRLA |
| C1 | 98.68 | 98.85 | **100.00** |
| C2 | 95.74 | 96.75 | **99.17** |
| C3 | 94.12 | 94.97 | **98.78** |
| C4 | 98.85 | 99.54 | 99.49 |
| C5 | 98.67 | 99.05 | 99.67 |
| C6 | 95.51 | 97.44 | 98.42 |
| C7 | 96.29 | 98.72 | 98.69 |
| C8 | 96.65 | 97.52 | 98.27 |
| C9 | 96.30 | 98.69 | 99.21 |
| C10 | 96.64 | 97.57 | 99.35 |
| C11 | 100.00 | 100.00 | 100.00 |
| C12 | 99.50 | 99.54 | 99.97 |
| C13 | 95.45 | 96.25 | **98.23** |
| C14 | 94.59 | 96.60 | **98.68** |
| C15 | 95.62 | 97.59 | 98.03 |
| C16 | 96.28 | 96.96 | 97.64 |
| C17 | 93.68 | 95.70 | **98.34** |
| C18 | 95.80 | 96.92 | 97.30 |
| C19 | 95.52 | 93.66 | **98.43** |
| C20 | 93.29 | 94.52 | **97.20** |
| C21 | 94.64 | 93.95 | **98.29** |
| C22 | 93.85 | 93.35 | **98.02** |
| C23 | 92.08 | 93.72 | **98.79** |
| C24 | 100.00 | 98.33 | 99.33 |
| C25 | 96.69 | 97.66 | 99.35 |
| **C26** | 94.58 | 96.83 | **98.34** |
| **C27** | 94.04 | 95.04 | **98.13** |

It can be observed that the accuracy of ITD & ResNet is the lowest, and over-fitting occurs at the end of training. ITD & RLA perform better, as RLA is an improved version of ResNet. Comparing different feature extraction methods, it can be found that EEMD and VMD have better feature extraction performance than ITD, but the test shows that they have a higher amount of computation, with each sample requiring 170.83 ms and 124.33 ms, respectively. This is because the variational mode needs to be solved by repetitive iterative, and EEMD requires a lot of interpolation calculations. The comparison between ITD & WRLA and ITD & RLA shows that WRLA maintains a stable advantage. Combining the proposed I-IVTD, I-IVTD & WRLA achieves the best performance among the listed frameworks.

### *D. Comparison with advanced frameworks*

To further verify the performance of the proposed framework, this section compares with the advanced frameworks reported in recent years. For fairness, the key parameters of the test are listed. The comparison is expanded from four dimensions: the number of disturbances, feature extraction method, SNR of the test signal, and detection accuracy. The best results reported by different advanced frameworks are listed in Table V, where 'Year' refers to the reported time of the frameworks, 'Manual' means manual design feature, and 'Auto' represents automatic frameworks.

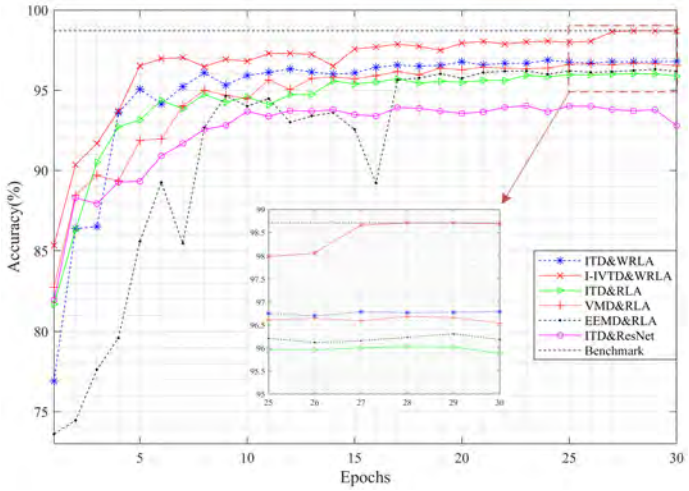


Fig. 7. The training process of different frameworks.

TABLE V
COMPARISON WITH THE EXISTING ADVANCED METHODS

| Framework (Year) | Num. of PQDs | Feature Extraction | SNR(dB) | Accuracy (%) |
|---|---|---|---|---|
| DWT+RF [23] (2020) | 21 | Manual | pure | 96.21 |
| ICEEMD&AdKNN [24] (2021) | 21 | Manual | 50 | 97.33 |
| DNN [26] (2019) | 16 | Auto | 20 | 98.13 |
| IHT&ResNet50 [27] (2022) | 28 | Manual | 30 | 97.18 |
| LGAN [28] (2022) | 48 | Auto | 20 | 96.85 |
| XAI [30] (2022) | 16 | Auto | 20 | 96.1 |
| ACMP&GOA-SVM [34] (2021) | 16 | Manual | 20 | 97.13 |
| **I-IVTD&WRLA** | **27** | **Auto** | **20** | **98.71** |

In Table V, all frameworks are designed to detect complex disturbances, but they differ in their ability to detect them. XAI [29] considers the interpretability of the judgment basis when detecting complex disturbances, but it has an average accuracy of only 96.1 %. LGAN [27] considers 48 types of disturbances, but its detection accuracy is relatively low. DNN [25] has an accuracy of over 98 % at 20 dB, but it can only identify 16 types of disturbances. The other methods require manual design of features [22] [23] [26] [34], and their detection accuracy is lower than 98 %. In contrast, our proposed framework can detect nonlinear disturbances and achieved an accuracy of 98.71 % at 20 dB SNR, indicating that our framework performs better than the other methods.

### *E. The test based on power quality analysis platform*

To verify the performance of the proposed framework in the given application, a test was conducted on a power quality analysis platform. The structure of the test platform is depicted in Fig. 8.

In this test, the PQDs signal was generated using Fluke 6105A. The disturbance signal was modulated in amplitude to $\pm$5V using an analog circuit and then converted into a digital signal using AD7606 at a sampling rate of 3.2 kHz. The data was then transmitted to a PC using a transmission

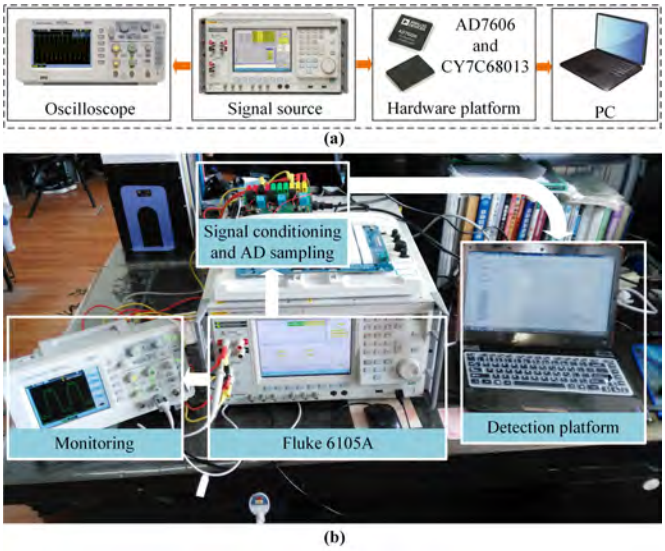


Fig. 8. The structure of power quality analysis platform. (a) Schematic of the signal sampling, (b) The hardware platform.

module with a maximum transmission rate of 480 Mbps. The transmission module also included an SRAM cache to prevent data loss. Finally, the disturbance signal was detected on the PC, which applied the proposed framework using C++. Due to the functional limitations of Fluke 6105A, only 12 types of power quality signals (C1, C2, C3, C4, C6, C7, C10, C11, C12, C21, C22, C23) were tested in this test. The test signal includes 6 types of single-disturbances, 3 types of 2-mixed disturbances, and 3 types of 3-mixed disturbances. Compared to existing frameworks, this section has conducted more comprehensive testing. The results are listed in Table VI.

TABLE VI
THE TEST RESULT IN POWER QUALITY ANALYSIS PLATFORM

| Class | Accuracy(%) | Class | Accuracy(%) | Average accuracy (%) | Test time per sample (ms) |
|---|---|---|---|---|---|
| C1 | 100.00 | C10 | 98.00 | | |
| C2 | 99.00 | C11 | 97.00 | | |
| C3 | 99.00 | C12 | 98.00 | 98.00 | 113.5 |
| C4 | 99.00 | C21 | 97.00 | | |
| C6 | 98.00 | C22 | 96.00 | | |
| C7 | 99.00 | C23 | 96.00 | | |

In Table VI, 100 tests were conducted for each type of disturbance. The results show that the detection accuracy based on the power quality disturbance experimental platform is lower than that of the simulation, as this is not an ideal experimental condition. However, the average accuracy still reaches 98.00 %. Each sample takes 113.5 ms, which is due to the additional time required for data transfer, but the proposed framework can still detect complex PQDs in real time. These results demonstrate that the proposed framework performs satisfactorily in experimental tests.

## VI. Conclusion

This paper proposes a novel framework for complex power quality disturbance detection based on I-IVTD and WRLA network. The proposed I-IVTD utilizes a variable time scale and multi-decomposition integration mechanism, which experiments show reduces mode aliasing and endpoint effects of ITD, and improves anti-noise performance. The proposed WRLA enhances the learning capabilities and accelerates the convergence of the network by adding weights to the feature maps. Under the premise of similar performance, WRLA reduced 77.4 thousand parameters than RLA. Simulation experiments demonstrate the advantages of the proposed framework, particularly in improving the robustness of the framework under non-linear perturbations. Compared to the unimproved framework, the accuracy improvement at 20 dB reaches 2.67 %. Additionally, the proposed framework outperforms existing methods, even under strong noise (98.71 % at 20 dB). Finally, experiments conducted on the experimental platform show that the processing time of each sample (duration 200 ms) only needs 113.5 ms, which means the proposed framework can detect complex power quality disturbances in real time with high accuracy.

However, this work still has limitations. I-IVTD still exists modal aliasing and endpoint effects, and detecting complex disturbances can only be done in frames with a period of 200 ms. In future works, the authors hope to further improve the performance of I-IVTD, seeking the more efficient CNN network and accurately detecting and locating the time span of disturbances. At the same time, it is also hoped that a sufficient number of disturbance signals can be collected in the power grid.

## References

[1] P. Roy, J. He, T. Zhao, and Y. V. Singh, "Recent advances of wind-solar hybrid renewable energy systems for power generation: A review," *IEEE Open J. Ind. Electron. Soc.*, vol. 3, pp. 81–104, 2022.
[2] D. L. Carní and F. Lamonaca, "Toward an automatic power quality measurement system: An effective classifier of power signal alterations," *IEEE Trans. Instrum. Meas.*, vol. 71, pp. 1–8, 2022.
[3] S. Elphick, P. Ciufo, G. Drury, V. Smith, S. Perera, and V. Gosbell, "Large scale proactive power-quality monitoring: An example from australia," *IEEE Trans. Power Del.*, vol. 32, no. 2, pp. 881–889, 2016.
[4] IEEE, "Ieee recommended practice for monitoring electric power quality; ieee std 1159-2009 (revision of ieee std 1159-1995)," 2009.
[5] F. A. Borges, R. A. Fernandes, I. N. Silva, and C. B. Silva, "Feature extraction and power quality disturbances classification using smart meters signals," *IEEE Trans. Ind. Inf.*, vol. 12, no. 2, pp. 824–833, 2015.
[6] J. Song, A. Mingotti, J. Zhang, L. Peretto, and H. Wen, "Fast iterative-interpolated dft phasor estimator considering out-of-band interference," *IEEE Trans. Instrum. Meas.*, vol. 71, pp. 1–14, 2022.
[7] K. Satpathi, Y. M. Yeap, A. Ukil, and N. Geddada, "Short-time fourier transform based transient analysis of vsc interfaced point-to-point dc system," *IEEE Trans. Ind. Electron.*, vol. 65, no. 5, pp. 4080–4091, 2018.
[8] K. Thirumala, M. S. Prasad, T. Jain, and A. C. Umarikar, "Tunable-q wavelet transform and dual multiclass svm for online automatic detection of power quality disturbances," *IEEE Trans. Smart Grid*, vol. 9, no. 4, pp. 3018–3028, 2018.
[9] M. D. Borrás, J. C. Bravo, and J. C. Montaño, "Disturbance ratio for optimal multi-event classification in power distribution networks," *IEEE Trans. Ind. Electron.*, vol. 63, no. 5, pp. 3117–3124, 2016.
[10] M. Venkateswara Reddy and R. Sodhi, "A modified s-transform and random forests-based power quality assessment framework," *IEEE Trans. Instrum. Meas.*, vol. 67, no. 1, pp. 78–89, 2018.

[11] J. Ma, J. Liu, W. Qiu, Q. Tang, Q. Wang, C. Li, L. Peretto, and Z. Teng, "An intelligent classification framework for complex pqds using optimized ks-transform and multiple fusion cnn," *IEEE Trans. Ind. Inf.*, pp. 1–10, 2023.
[12] M. Sahani and P. K. Dash, "Automatic power quality events recognition based on hilbert huang transform and weighted bidirectional extreme learning machine," *IEEE Trans. Ind. Inf.*, vol. 14, no. 9, pp. 3849–3858, 2018.
[13] R. Wang, W. Huang, B. Hu, Q. Du, and X. Guo, "Harmonic detection for active power filter based on two-step improved eemd," *IEEE Trans. Instrum. Meas.*, vol. 71, pp. 1–10, 2022.
[14] C. Zhao and et al., "Novel method based on variational mode decomposition and a random discriminative projection extreme learning machine for multiple power quality disturbance recognition," *IEEE Trans. Ind. Inf.*, vol. 15, no. 5, pp. 2915–2926, 2018.
[15] P. D. Achlerkar, S. R. Samantaray, and M. Sabarimalai Manikandan, "Variational mode decomposition and decision tree based detection and classification of power quality disturbances in grid-connected distributed generation system," *IEEE Trans. Smart Grid*, vol. 9, no. 4, pp. 3122–3132, 2018.
[16] N. E. Huang, *Hilbert-Huang transform and its applications*. World Scientific, 2014, vol. 16.
[17] J. Liu, H. Song, H. Sun, and H. Zhao, "High-precision identification of power quality disturbances under strong noise environment based on fastica and random forest," *IEEE Trans. Ind. Inf.*, vol. 17, no. 1, pp. 377–387, 2021.
[18] Y. Wang, Q. Li, F. Zhou, Y. Zhou, and X. Mu, "A new method with hilbert transform and slip-svd-based noise-suppression algorithm for noisy power quality monitoring," *IEEE Trans. Instrum. Meas.*, vol. 68, no. 4, pp. 987–1001, 2018.
[19] G. W. Chang, Y.-Y. Chen, and Y.-L. Lin, "A synchrosqueezing transform-based hybrid method for voltage fluctuations assessment," *IEEE Trans. Power Delivery*, vol. 33, no. 5, pp. 2541–2550, 2018.
[20] D. Pattanaik, S. C. Swain, I. S. Samanta, U. K. Rout, R. Dash, and K. Swain, "Synchrosqueezed wavelet transform based power quality disturbance detection and monitoring of solar integrated micro-grid," in *ICPEE 2023*, 2023, pp. 1–6.
[21] M. Valtierra-Rodriguez, R. de Jesus Romero-Troncoso, R. A. Osornio-Rios, and A. Garcia-Perez, "Detection and classification of single and combined power quality disturbances using neural networks," *IEEE Trans. Ind. Electron.*, vol. 61, no. 5, pp. 2473–2482, 2014.
[22] Z. Liu, Y. Cui, and W. Li, "A classification method for complex power quality disturbances using eemd and rank wavelet svm," *IEEE Trans. Smart Grid*, vol. 6, no. 4, pp. 1678–1685, 2015.
[23] M. Markovska, D. Taskovski, Z. Kokolanski, V. Dimchev, and B. Velkovski, "Real-time implementation of optimized power quality events classifier," *IEEE Trans. Ind. Appl.*, vol. 56, no. 4, pp. 3431–3442, 2020.
[24] Y. Liu, T. Jin, M. A. Mohamed, and Q. Wang, "A novel three-step classification approach based on time-dependent spectral features for complex power quality disturbances," *IEEE Trans. Instrum. Meas.*, vol. 70, pp. 1–14, 2021.
[25] Y. Luo, K. Li, Y. Li, D. Cai, C. Zhao, and Q. Meng, "Three-layer bayesian network for classification of complex power quality disturbances," *IEEE Trans. Ind. Inf.*, vol. 14, no. 9, pp. 3997–4006, 2018.
[26] S. Wang and H. Chen, "A novel deep learning method for the classification of power quality disturbances using deep convolutional neural network," *Appl. Energy*, vol. 235, pp. 1126–1140, 2019.
[27] D. Yuan, Y. Liu, M. Lan, T. Jin, and M. A. Mohamed, "A novel recognition method for complex power quality disturbances based on visualization trajectory circle and machine vision," *IEEE Trans. Instrum. Meas.*, vol. 71, pp. 1–13, 2022.
[28] D. Gu, Y. Gao, Y. Li, Y. Zhu, and C. Wu, "A novel label-guided attention method for multilabel classification of multiple power quality disturbances," *IEEE Trans. Ind. Inf.*, vol. 18, no. 7, pp. 4698–4706, 2022.
[29] G. Feng and K.-W. Lao, "Wasserstein adversarial learning for identification of power quality disturbances with incomplete data," *IEEE Trans. Ind. Inf.*, 2023.
[30] R. Machlev, M. Perl, J. Belikov, K. Y. Levy, and Y. Levron, "Measuring explainability and trustworthiness of power quality disturbances classifiers using xai—explainable artificial intelligence," *IEEE Trans. Ind. Inf.*, vol. 18, no. 8, pp. 5127–5137, 2022.
[31] M. G. Frei and I. Osorio, "Intrinsic time-scale decomposition: time–frequency–energy analysis and real-time filtering of non-stationary signals," *Proceedings of the Royal Society A: Mathematical, Physical and Engineering Sciences*, vol. 463, no. 2078, pp. 321–342, 2007.
[32] J. Zhao, Y. Fang, and G. Li, "Recurrence along depth: Deep convolutional neural networks with recurrent layer aggregation," *Advances in Neural Information Processing Systems*, vol. 34, pp. 10 627–10 640, 2021.
[33] R. Machlev, A. Chachkes, J. Belikov, Y. Beck, and Y. Levron, "Open source dataset generator for power quality disturbances with deep-learning reference classifiers," *Electr. Power Syst. Res.*, vol. 195, p. 107152, 2021.
[34] S. Z. Motlagh and A. A. Foroud, "Power quality disturbances recognition using adaptive chirp mode pursuit and grasshopper optimized support vector machines," *Measurement*, vol. 168, p. 108461, 2021.

**Kunzhi Zhu** received the B.Sc. degree in measurement and control technology and instrument from Hunan University, Changsha, China, in 2018.

He is currently working toward the Ph.D. degree in electrical engineering, Hunan University, Changsha, China. His research interests include signal processing, machine learning, power system analysis, cyber-security of synchrophasor and mechanical fault diagnosis.

**Zhaosheng Teng** was born in Hunan, China, in 1963. He received the B.Sc., M.Sc., and Ph.D. degrees from Hunan University, Hunan, in 1984, 1995, and 1998, respectively, all in electrical engineering. He was a Post-Doctoral Research Fellow with the National University of Defense Technology, Hunan, from 1998 to 2000. Since 2000, he has been a Professor with Hunan University.

His current research interests include power quality monitoring, information fusion, and electrical measurement.

**Wei Qiu** (Member, IEEE) received the B.Sc. degree in electrical engineering from Hubei University of Technology, Wuhan, China, in 2015, and the M.Sc. and Ph.D. degrees in electrical engineering from Hunan University, Changsha, China, in 2017 and 2021, respectively. He was also a joint Doctoral student with the University of Tennessee from 2019 to 2021. He was a Research Associate in the Department of Electrical Engineering and Computer Science, The University of Tennessee, Knoxville, TN, USA from 2021 to 2022. He is currently a Research Associate in the College of Electrical and Information Engineering, Hunan University.

His current research interests include situational awareness, cyber-security of synchrophasor, power quality measurement, and reliability analysis of power equipment.

**Alessandro Mingotti** (S'17) was born in Cento (FE), Italy in 1992. He received the B.S., M.S., and Ph.D. degrees in electrical engineering from the University of Bologna, Bologna, Italy, in 2014, 2016, and 2020, respectively.

He is a Senior Assistant Professor at the University of Bologna from 2021. His research interests include management and condition maintenance of distribution networks, development, modelling, and metrological characterization of instrument transformers. He is also working on several National and European funded Projects.

**Qiu Tang** was born in Hunan, China, in 1970. She received the B.Sc., M.Sc., and Ph.D. degrees in electrical engineering from Hunan University, Changsha, China, in 1992, 1995, and 2010, respectively, and the M.Sc. degree in electrical engineering from the University of Nottingham, Nottingham, U.K., in 2005.

She has been an Associate Professor at Hunan University since 2006. Her current research interests include power system analysis, digital signal processing, and virtual instruments.

**Wenxuan Yao** (Senior Member, IEEE) received his B.Sc. and Ph.D. degrees from the College of Electrical and Information Engineering, Hunan University, Changsha, China, in 2011 and 2017, respectively and the Ph.D. degree from Department of Electrical Engineering and Computer Science, University of Tennessee, Knoxville, USA, in 2018.

He is currently a professor and Ph.D. supervisor at Hunan University. His main research interest includes smart grid, wide-area synchrophasor measurement technology and its application, and power quality monitoring.